Publications

8-29-2009

Waves in Inhomogeneous Solids

Arkadi Berezovski
Tallinn University of Technology, arkadi.berezovski@cs.ioc.ee

Mihhail Berezovski
Tallinn University of Technology, berezovm@erau.edu

Juri Engelbrecht
Tallinn University of Technology, je@ioc.ee

Scholarly Commons Citation

Waves in Inhomogeneous Solids

Arkadi Berezovski, Mihhail Berezovski and Jüri Engelbrecht

Abstract The paper aims at presenting a numerical technique used in simulating the propagation of waves in inhomogeneous elastic solids. The basic governing equations are solved by means of a finite-volume scheme that is faithful, accurate, and conservative. Furthermore, this scheme is compatible with thermodynamics through the identification of the notions of numerical fluxes (a notion from numerics) and of excess quantities (a notion from irreversible thermodynamics). A selection of one-dimensional wave propagation problems is presented, the simulation of which exploits the designed numerical scheme. This selection of exemplary problems includes (i) waves in periodic media for weakly nonlinear waves with a typical formation of a wave train, (ii) linear waves in laminates with the competition of different length scales, (iii) nonlinear waves in laminates under an impact loading with a comparison with available experimental data, and (iv) waves in functionally graded materials.

1 Introduction

Waves correspond to continuous variations of the states of material points representing a medium. The characteristic feature of waves is their motion. In mechanics the motion of waves is governed by the conservation laws for mass, linear momentum, and energy. These conservation laws, complemented by constitutive relations, are the basis of the theory of thermoelastic waves in solids [1, 3, 9, 19].

Inhomogeneous solids include layered and randomly reinforced composites, multiphase and polycrystalline alloys, functionally graded materials, ceramics and polymers with certain microstructure, etc. Therefore, it is impossible to present a complete theory of linear and nonlinear wave propagation for the full diversity of

Centre for Nonlinear Studies, Institute of Cybernetics at Tallinn University of Technology, Akadeemia tee 21, 12618 Tallinn, Estonia, e-mail: arkadi.berezovski@cs.ioc.ee

possible situations, in so far as geometry, contrast of multiphase properties and loading conditions are concerned.

From a practical point of view, we need to perform numerical calculations. Many numerical methods have been proposed to compute wave propagation in heterogeneous solids, among them, the stiffness matrix recursive algorithm [33, 38] and the spectral layer element method [10, 11] should be mentioned, in addition to more common finite-element, finite-difference, and finite-volume methods.

Here the general idea is the following: division of a body into a finite number of computational cells requires the description of all fields inside the cells as well as the interaction between neighboring cells. Approximation of wanted fields inside the cells leads to discontinuities of the fields at the boundaries between cells. This also leads to the appearance of excess quantities, which represent the difference between the exact and approximate values of the fields. Interaction between neighboring cells is described by means of fluxes at the boundaries of the cells. These fluxes correspond to the excess quantities and, therefore, can be calculated by means of jump relations at the boundaries between cells.

In this paper, we demonstrate how the finite-volume wave-propagation algorithm developed in [27] can be reformulated in terms of the excess quantities and then applied to the wave propagation in inhomogeneous solids. Both original and modified algorithms are stable, high-order accurate, thermodynamically consistent, and applicable both to linear and nonlinear waves.

1.1 Governing equations

The simplest example of heterogeneous media is a periodic medium composed by materials with different properties. One-dimensional wave propagation in the framework of linear elasticity is governed by the conservation of linear momentum [1]

$$\rho(x)\frac{\partial v}{\partial t} - \frac{\partial \sigma}{\partial x} = 0, \tag{1}$$

and the kinematic compatibility condition

$$\frac{\partial \varepsilon}{\partial t} = \frac{\partial v}{\partial x}. \tag{2}$$

Here t is time, x is the space variable, the particle velocity $v = u_t$ is the time derivative of the displacement u, the one-dimensional strain $\varepsilon = u_x$ is the space derivative of the displacement, σ is the Cauchy stress, and ρ is the material density. The compatibility condition (2) follows immediately from the definitions of the strain and the particle velocity.

The two equations (1) and (2) contain three unknowns: v, σ and ε.

The closure of the system of equations (1) and (2) is achieved by a constitutive relation, which in the simplest case is Hooke's law

$$\sigma = \rho(x)c^2(x)\varepsilon, \tag{3}$$

where $c(x) = \sqrt{(\lambda(x) + 2\mu(x))/\rho(x)}$ is the corresponding longitudinal wave velocity, and $\lambda(x)$ and $\mu(x)$ are the so-called Lamé coefficients. The indicated explicit dependence on the point x means that the medium is materially inhomogeneous.

The system of equations (1)–(3) can be expressed in the form of a conservation law

$$\frac{\partial}{\partial t}q(x,t) + \frac{\partial}{\partial x}f(q(x,t)) = 0, \tag{4}$$

with

$$q(x,t) = \begin{pmatrix} \varepsilon \\ \rho v \end{pmatrix} \quad \text{and} \quad f(x,t) = \begin{pmatrix} -v \\ -\rho c^2 \varepsilon \end{pmatrix}. \tag{5}$$

In the linear case, equation (4) can be rewritten in the form

$$\frac{\partial}{\partial t}q(x,t) + A\frac{\partial}{\partial x}q(x,t) = 0, \tag{6}$$

where the matrix A is given by

$$A = \begin{pmatrix} 0 & -1/\rho \\ -\rho c^2 & 0 \end{pmatrix}. \tag{7}$$

We will solve the system of equations (1)–(3) numerically. Although a numerical solution can be difficult with standard methods, high-resolution finite volume methods based on solving Riemann problems have been found to perform very well on linear hyperbolic systems modeling wave propagation in rapidly-varying heterogeneous media [16].

2 The wave-propagation algorithm

Standard methods cannot give high accuracy near discontinuities in the material parameters and will often fail completely in problems where the parameters vary drastically on the grid scale. By contrast, solving the Riemann problem at each cell interface properly resolves the solution into waves, taking into account every discontinuity in the parameters, and automatically handling the reflection and transmission of waves at each interface. This is crucial in developing the correct macroscopic behavior. As a result, Riemann-solver methods are quite natural for this application. Moreover, the methods extend easily from linear to nonlinear problems. Expositions of such methods and pointers to the rich literature base can be found in many sources [17, 20, 27, 36, 37].

2.1 Averaged quantities

Let us introduce a computational grid of cells $C_n = [x_{n-1/2}, x_{n+1/2}]$ with interfaces $x_{n-1/2} = (n-1)/2\Delta x$ and time levels $t_k = k\Delta t$. For simplicity, the grid size Δx and time step Δt are assumed to be constant. Integrating equation (4) over $C_n \times [t_k, t_{k+1}]$ gives

$$\int_{x_{n-1/2}}^{x_{n+1/2}} q(x, t_{k+1})dx = \int_{x_{n-1/2}}^{x_{n+1/2}} q(x, t_k)dx - \tag{8}$$

$$- \left(\int_{t_k}^{t_{k+1}} f(q(x_{n+1/2}, t))dt - \int_{t_k}^{t_{k+1}} f(q(x_{n-1/2}, t))dt \right).$$

Introducing the average Q_n of the exact solution on C_n at time $t = t_k$ and the numerical flux F_n that approximates the time average of the exact flux taken at the interface between the cells C_{n-1} and C_n, i.e.

$$Q_n \approx \frac{1}{\Delta x} \int_{x_{n-1/2}}^{x_{n+1/2}} q(x, t_k)dx, \quad F_n \approx \frac{1}{\Delta t} \int_{t_k}^{t_{k+1}} f(q(x_{n-1/2}, t))dt, \tag{9}$$

we can rewrite equation (8) in the form of a numerical method in the flux-differencing form

$$Q_n^{k+1} = Q_n^k - \frac{\Delta t}{\Delta x}(F_{n+1}^k - F_n^k). \tag{10}$$

In general, however, we cannot evaluate the time integrals on the right-hand side of equation (8) exactly, since $q(x_{n\pm1/2}, t)$ varies with time along each edge of the cell, and we do not have the exact solution to work with. If we can approximate this average flux based on the values Q^k, then we will have a fully-discrete method.

2.2 Numerical fluxes

Numerical fluxes are determined by means of the solution of the Riemann problem at interfaces between cells. The solution of the Riemann problem (at the interface between cells $n-1$ and n) consists of two waves, which we denote, following [27], $\mathcal{W}_n^I$ and $\mathcal{W}_n^{II}$. The left-going wave $\mathcal{W}_n^I$ moves into cell $n-1$, and the right-going wave $\mathcal{W}_n^{II}$ moves into cell n. The state between the two waves must be continuous across the interface (Rankine-Hugoniot condition) [27]:

$$\mathcal{W}_n^I + \mathcal{W}_n^{II} = Q_n - Q_{n-1}. \tag{11}$$

In the linear case, the considered waves are determined by eigenvectors of the matrix A [27]:

$$\mathcal{W}_n^I = \gamma_n^I r_{n-1}^I, \quad \mathcal{W}_n^{II} = \gamma_n^{II} r_n^{II}. \tag{12}$$

This means that equation (11) is represented as

$$\gamma_n^I r_{n-1}^I + \gamma_n^{II} r_n^{II} = Q_n - Q_{n-1}. \tag{13}$$

Considering the definition of eigenvectors $Ar = \lambda r$, we see that the eigenvector

$$r^I = \begin{pmatrix} 1 \\ \rho c \end{pmatrix} \tag{14}$$

corresponds to the eigenvalue $\lambda^I = -c$ (left-going wave). Similarly, the eigenvector

$$r^{II} = \begin{pmatrix} 1 \\ -\rho c \end{pmatrix} \tag{15}$$

corresponds to the eigenvalue $\lambda^{II} = c$ (right-going wave). Substituting the eigenvectors into equation (13), we have

$$\gamma_n^I \begin{pmatrix} 1 \\ \rho_{n-1} c_{n-1} \end{pmatrix} + \gamma_n^{II} \begin{pmatrix} 1 \\ -\rho_n c_n \end{pmatrix} = Q_n - Q_{n-1}, \tag{16}$$

or, more explicitly,

$$\begin{pmatrix} 1 & 1 \\ \rho_{n-1} c_{n-1} & -\rho_n c_n \end{pmatrix} \begin{pmatrix} \gamma_n^I \\ \gamma_n^{II} \end{pmatrix} = \begin{pmatrix} \bar{\varepsilon}_n - \bar{\varepsilon}_{n-1} \\ \rho \bar{v}_n - \rho \bar{v}_{n-1} \end{pmatrix}. \tag{17}$$

Solving the system of linear equations (17), we obtain the amplitudes of the left-going and right-going waves. Then the numerical fluxes in the Godunov-type numerical scheme are determined as follows:

$$F_{n+1}^k = -\lambda_{n+1}^I \mathcal{W}_{n+1}^I = -c_{n+1} \gamma_{n+1}^I r_n^I, \tag{18}$$

$$F_n^k = \lambda_n^{II} \mathcal{W}_n^{II} = -c_n \gamma_n^{II} r_n^{II}. \tag{19}$$

Finally, the Godunov-type scheme is expressed in the form

$$Q_n^{k+1} = Q_n^k + \frac{\Delta t}{\Delta x} \left(c_{n+1} \gamma_{n+1}^I r_n^I - c_n \gamma_n^{II} r_n^{II} \right). \tag{20}$$

This is the standard form for the wave-propagation algorithm [27].

Within the wave-propagation algorithm, every discontinuity in parameters is taken into account by solving the Riemann problem at each interface between discrete elements. The reflection and transmission of waves at each interface are handled automatically for the considered inhomogeneous media.

2.3 Second-order corrections

The scheme considered above is formally first-order accurate only. To increase the order of accuracy, we rewrite the numerical scheme as

$$Q_n^{k+1} = Q_n^k + \Delta_n^{up} - \frac{\Delta t}{\Delta x}(\tilde{F}_{n+1}^k - \tilde{F}_n^k), \tag{21}$$

where Δ_n^{up} equals the upwind flux (or Godunov flux) obtained from equation (20).

The term $\tilde{F}_n$ is used to update the solution so that second order accuracy is achieved. The flux for the second-order Lax-Wendroff scheme may be written as the Godunov flux plus a correction [27],

$$F_n = \frac{1}{2}A(Q_n + Q_{n-1}) - \frac{\Delta t}{2\Delta x}A(Q_n - Q_{n+1}) = F_n^G + \frac{1}{2}|A|\left(1 - \frac{\Delta t}{\Delta x}|A|\right)\Delta Q_n, \tag{22}$$

where $|A| = A^+ - A^-$. Hence, a natural choice for $\tilde{F}$ is

$$\tilde{F}_n = \frac{1}{2}|A|\left(1 - \frac{\Delta t}{\Delta x}|A|\right)\Delta Q_n = \frac{1}{2}\sum_p |\lambda^p|\left(1 - \frac{\Delta t}{\Delta x}|\lambda^p|\right)\mathcal{W}_n^p. \tag{23}$$

The Godunov-type scheme exhibits strong numerical dissipation, and discontinuities in the solution are smeared, causing low accuracy. The Lax-Wendroff scheme, on the other hand, is more accurate in smooth parts of the solution. However, near discontinuities, numerical dispersion generates oscillations, also reducing the accuracy. A successful approach to suppress these oscillations is to apply flux limiters [16, 23, 24, 25].

2.4 The conservative wave propagation algorithm

For the conservative wave-propagation algorithm [2], the solution of the generalized Riemann problem is obtained by using the decomposition of the flux difference $f_n(Q_n) - f_{n-1}(Q_{n-1})$ instead of the decomposition (11):

$$\mathcal{L}_n^I + \mathcal{L}_n^{II} = f_n(Q_n) - f_{n-1}(Q_{n-1}). \tag{24}$$

The waves $\mathcal{L}^I$ and $\mathcal{L}^{II}$ are still proportional to the eigenvectors of the matrix A

$$\mathcal{L}_n^I = \beta_n^I r_{n-1}^I, \quad \mathcal{L}_n^{II} = \beta_n^{II} r_n^{II}, \tag{25}$$

and the corresponding numerical scheme has the form

$$Q_n^{l+1} - Q_n^l = -\frac{\Delta t}{\Delta x}\left(\mathcal{L}_n^{II} + \mathcal{L}_{n+1}^I\right). \tag{26}$$

The coefficients β^I and β^{II} are determined from the solution of the system of linear equations

$$\begin{pmatrix} 1 & 1 \\ \rho_{n-1}c_{n-1} & -\rho_n c_n \end{pmatrix} \begin{pmatrix} \beta_n^I \\ \beta_n^{II} \end{pmatrix} = \begin{pmatrix} -(\bar{v}_n - \bar{v}_{n-1}) \\ -(\rho c^2 \bar{\varepsilon}_n - \rho c^2 \bar{\varepsilon}_{n-1}) \end{pmatrix}. \tag{27}$$

As it is shown in [2], the obtained algorithm is conservative and second-order accurate on smooth solutions.

3 Excess quantities and numerical fluxes

We could simply apply the numerical scheme described in the previous sections to simulate the wave propagation in periodic media. However, the splitting of the body into a finite number of computational cells and averaging all the fields over the cell volumes leads to a situation known in thermodynamics as "endoreversible system" [22]. This means that even if the state of each computational cell can be associated with a corresponding local equilibrium state (and, therefore, temperature and entropy can be defined as usual), the state of the whole body is a non-equilibrium one. The computational cells interact with each other, which leads to the appearance of excess quantities.

In the admitted non-equilibrium description [32], both stress and velocity are represented as the sum of the averaged (local equilibrium) and excess parts:

$$\sigma = \bar{\sigma} + \Sigma, \quad v = \bar{v} + \mathcal{V}. \tag{28}$$

Here $\bar{\sigma}$ and $\bar{v}$ are averaged fields and Σ and $\mathcal{V}$ are the corresponding excess quantities.

Therefore, we rewrite a first-order Godunov-type scheme (10) in terms of the excess quantities

$$(\rho \bar{v})_n^{k+1} - (\rho \bar{v})_n^k = \frac{\Delta t}{\Delta x} \left(\Sigma_n^+ - \Sigma_n^- \right), \tag{29}$$

$$\bar{\varepsilon}_n^{k+1} - \bar{\varepsilon}_n^k = \frac{\Delta t}{\Delta x} \left(\mathcal{V}_n^+ - \mathcal{V}_n^- \right). \tag{30}$$

Here an overbar denotes averaged quantities, a superscript k denotes a time step, a subscript n denotes the number of the computational cell, while Δt and Δx are time step and space step, respectively.

Though excess quantities are determined formally everywhere inside computational cells, we need to know only their values at the boundaries of the cells, where they play the role of numerical fluxes. To determine the values of the excess quantities at the boundaries between computational cells, we apply the jump relation for the linear momentum [6], which is reduced in the isothermal case to

$$[\bar{\sigma} + \Sigma] = 0. \tag{31}$$

Similarly, the jump relation following from the kinematic compatibility (2) reads

$$[\bar{v} + \mathcal{V}] = 0. \tag{32}$$

It should be noted that the two last jump conditions can be considered as the *continuity of genuine unknown fields* at the boundaries between computational cells, which is illustrated in Fig. 1.
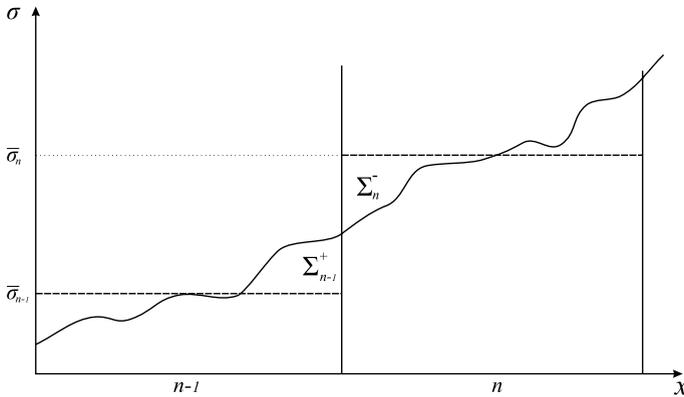

Fig. 1 Stresses in the bulk.

The values of the excess stresses and excess velocities at the boundaries between computational cells are not independent [8]. Considering Riemann invariants at the interface between computational cells, one can see that

$$\rho_n c_n \mathcal{V}_n^- + \Sigma_n^- \equiv 0, \tag{33}$$

$$\rho_{n-1} c_{n-1} \mathcal{V}_{n-1}^+ - \Sigma_{n-1}^+ \equiv 0, \tag{34}$$

i.e., the excess quantities depend on each other at the cell boundary.

3.1 Excess quantities at the boundaries between cells

Rewriting the jump relations (31), (32) in the form

$$(\Sigma^+)_{n-1} - (\Sigma^-)_n = (\bar{\sigma})_n - (\bar{\sigma})_{n-1}, \tag{35}$$

$$(\mathcal{V}^+)_{n-1} - (\mathcal{V}^-)_n = (\bar{v})_n - (\bar{v})_{n-1}, \tag{36}$$

and using the dependence between excess quantities (equations (33) and (34)),

we obtain then the system of linear equations for the determination of the excess velocities

$$\mathcal{V}_{n-1}^+ - \mathcal{V}_n^- = \bar{v}_n - \bar{v}_{n-1}, \tag{37}$$

$$\mathcal{V}_{n-1}^+ \rho_{n-1} c_{n-1} + \mathcal{V}_n^- \rho_n c_n = \rho_n c_n^2 \bar{\varepsilon}_n - \rho_{n-1} c_{n-1}^2 \bar{\varepsilon}_{n-1}. \tag{38}$$

In matrix notation the latter system of equations has the form

$$\begin{pmatrix} 1 & 1 \\ \rho_{n-1} c_{n-1} & -\rho_n c_n \end{pmatrix} \begin{pmatrix} -\mathcal{V}_{n-1}^+ \\ \mathcal{V}_n^- \end{pmatrix} = \begin{pmatrix} -(\bar{v}_n - \bar{v}_{n-1}) \\ -(\rho c^2 \bar{\varepsilon}_n - \rho c^2 \bar{\varepsilon}_{n-1}) \end{pmatrix}. \tag{39}$$

Comparing the obtained equation with equation (30), we conclude that

$$\beta_n^I = -\mathcal{V}_{n-1}^+, \quad \beta_n^{II} = \mathcal{V}_n^-. \tag{40}$$

This means that the excess quantities following from non-equilibrium jump relations at the boundary between computational cells correspond to the numerical fluxes in the conservative wave-propagation algorithm.

The representation of the wave-propagation algorithm in terms of the excess quantities given here is formally identical to its conservative form [2]. The advantage of the new representation manifests itself at discontinuities, for which jump relations cannot be reduced to the continuity of true values, e.g., at phase-transition fronts or cracks.

4 One-dimensional waves in periodic media

As the first example, we consider the propagation of a pulse in a periodic medium. The initial form of the pulse is given in Fig. 2, where the periodic variation in density is also shown by dashed lines. For the test problem, the materials are chosen as polycarbonate ($\rho = 1190$ kg/m^3, $c = 4000$ m/s) and Al 6061 ($\rho = 2703$ kg/m^3, $c = 6149$ m/s).

We apply the numerical scheme (29) and (30) for the solution of the system of equations (1)–(3). The corresponding excess quantities are calculated by means of equations (35)–(38).

As it was noted, we can exploit all the advantages of the wave-propagation algorithm, including second-order corrections and transversal propagation terms [24]. However, no limiters are used in the calculations. Suppressing spurious oscillations is achieved by means of using a first-order Godunov step after each three second-order Lax-Wendroff steps. This idea of composition was invented in [29].

Calculations are performed with Courant-Friedrichs-Levy number equal to 1. The simulation result for 4000 time steps is shown in Fig. 3.

We observe a distortion of the pulse shape and a decrease in the velocity of the pulse propagation in comparison to the maximal longitudinal wave velocity in the materials. These results correspond to the prediction of the effective media theory [34] both qualitatively and quantitatively [16].
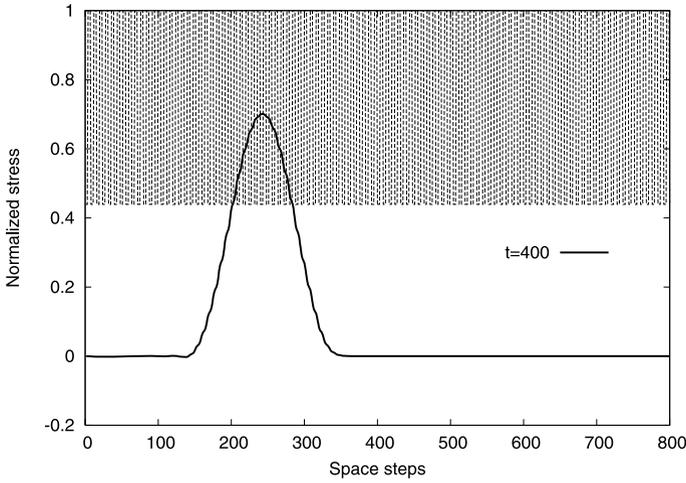
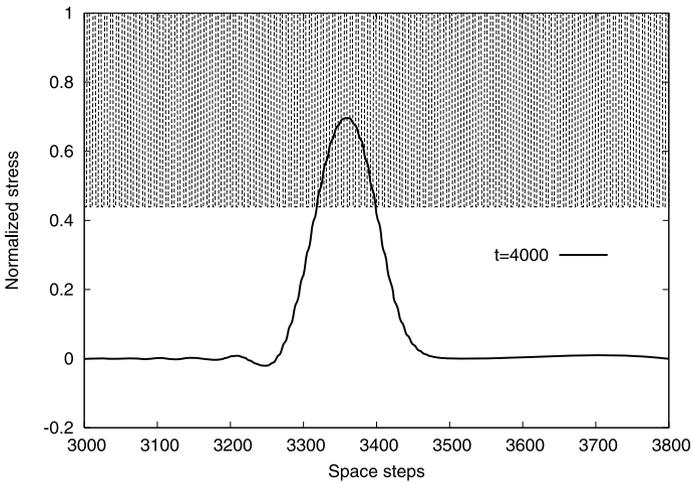**Fig. 2** Initial pulse shape. Reproduced from [5].

Fig. 3 Pulse shape at time step 4000. Reproduced from [5].

It should be noted that the effective media theory [34] leads to the dispersive wave equation

$$\frac{\partial^2 u}{\partial t^2} = (c^2 - c_a^2)\frac{\partial^2 u}{\partial x^2} + p^2 c_a^2 c_b^2 \frac{\partial^4 u}{\partial x^4}, \tag{41}$$

where u is the displacement, p is the periodicity parameter, and c_a and c_b are parameters of the effective media [15], instead of the wave equation following from equations (1)–(3)

$$\frac{\partial^2 u}{\partial t^2} = c^2 \frac{\partial^2 u}{\partial x^2}. \tag{42}$$

Equation (41) exhibits both *dispersion* (fourth-order space derivative) and the alteration in the longitudinal wave speed.

5 One-dimensional weakly nonlinear waves in periodic media

In the next example, we will see the influence of the materials' nonlinearity on the wave propagation. To close the system of equations (1) and (2) in the case of weakly nonlinear media we apply a simple nonlinear stress-strain relation

$$\sigma = \rho c^2 \varepsilon (1 + B\varepsilon), \tag{43}$$

where B is a parameter of nonlinearity, the values and sign of which are supposed to be different for hard and soft materials.
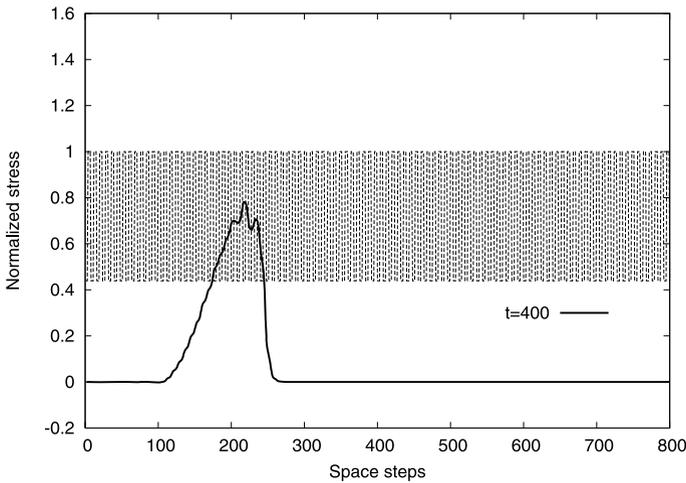

Fig. 4 Pulse shape at time step 400. Nonlinear case.

The solution method is almost the same as before. The approximate Riemann solver for the nonlinear elastic media (equation (43)) is similar to that used in [26, 28]. A modified longitudinal wave velocity $\hat{c}$, following the nonlinear stress-strain relation (43), is applied at each time step in the numerical scheme (29) and (30):

$$\hat{c} = c\sqrt{1 + 2B\varepsilon} \tag{44}$$

instead of the piecewise constant one corresponding to the linear case.

We consider the same pulse shape and the same materials (polycarbonate and Al 6061) as in the case of the linear periodic medium. However, the nonlinear effects appear only for a sufficiently high magnitude of loading. The values of the parameter of nonlinearity B were chosen as 0.24 for Al 6061 and 0.8 for polycarbonate.

The results of the simulations corresponding to 400, 1600, and 5200 time steps are shown in Figs. 4–6.
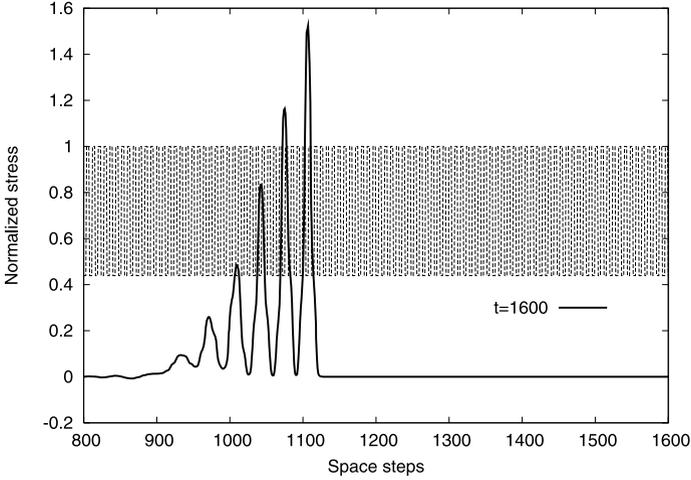

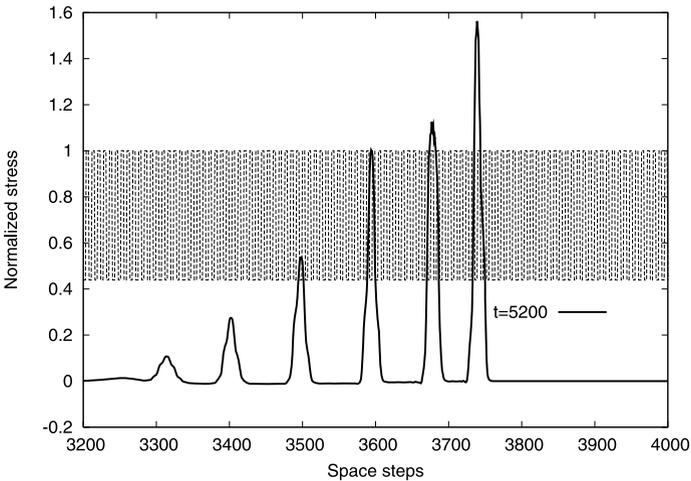**Fig. 5** Pulse shape at time step 1600. Nonlinear case.

Fig. 6 Pulse shape at time step 5200. Nonlinear case. Reproduced from [5].

We observe that an initial bell-shaped pulse is transformed into a train of soliton-like pulses propagating with amplitude-dependent speeds. Such kind of behavior was first reported in [26], where these pulses were called "stegotons" because their shape is influenced by the periodicity.

In principle, the soliton-like solution could be expected because if we combine the weak nonlinearity (43) with the dispersive wave equation in terms of the effective media theory (41), we arrive at the Boussinesq-type equation

$$\frac{\partial^2 u}{\partial t^2} = (c^2 - c_a^2)\frac{\partial^2 u}{\partial x^2} + \alpha B \frac{\partial u}{\partial x}\frac{\partial^2 u}{\partial x^2} + p^2 c_a^2 c_b^2 \frac{\partial^4 u}{\partial x^4}, \qquad (45)$$

which possesses soliton-like solutions.

6 One-dimensional linear waves in laminates

There are three basic length scales in wave propagation phenomena:

- the typical wavelength λ;
- the typical size of the inhomogeneities d;
- the typical size of the whole inhomogeneity domain l.

In the case of infinite periodic media considered above the third length scale was absent. Therefore, it may be instructive to consider wave propagation in a body where the periodic arrangement of layers of different materials is confined within a finite spatial domain.
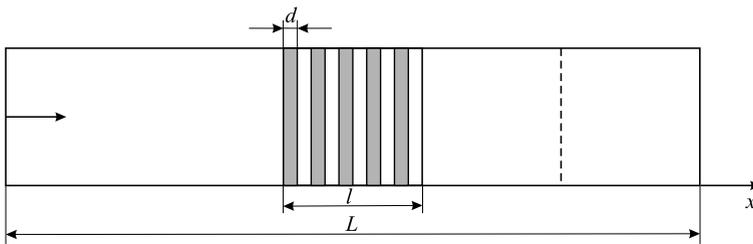

Fig. 7 Length scales in laminate.

To investigate the influence of the size of the inhomogeneity domain, we compare the shape of the pulse in the homogeneous medium with the corresponding pulse transmitted through the periodic array with a different number of distinct layers (Fig. 7).

We use Ti ($\rho = 4510$ kg/m^3, $c = 5020$ m/s) and Al ($\rho = 2703$ kg/m^3, $c = 5240$ m/s) as materials in the distinct layers in the numerical simulations of linear elastic wave propagation.

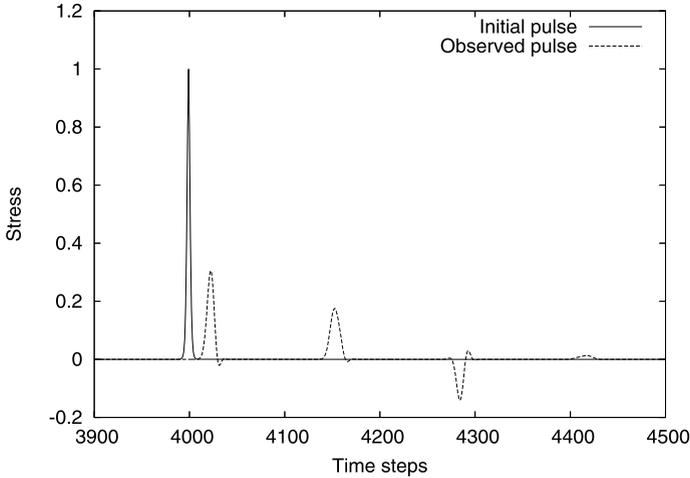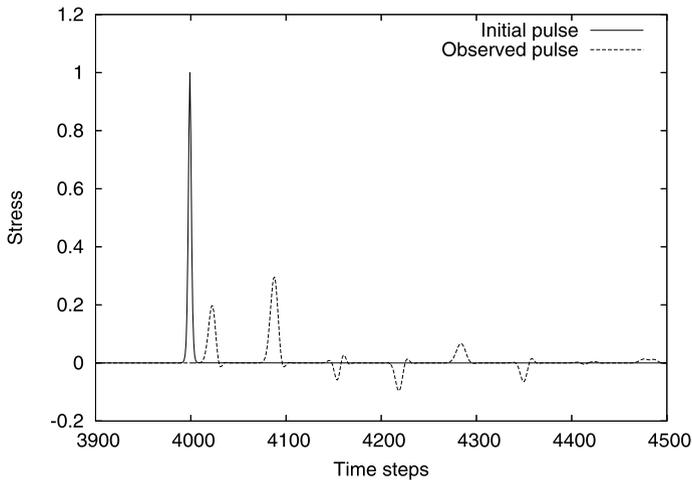**Fig. 8** Pulse shape at 4000 time steps ($d = 64\triangle x, l = 1000\triangle x$).

Fig. 9 Pulse shape at 4000 time steps ($d = 32\triangle x, l = 1000\triangle x$).

We apply a stress pulse, the width λ of which corresponds to $30\triangle x$ ($\triangle x$ is the space step)

$$\sigma(t) = \frac{2}{\cosh^2(0.5(t - 15\triangle t))} \qquad (46)$$

at the left end of the domain (Fig. 7), and record the resulting pulse at $x = 4000\triangle x$. The location is indicated by the dashed line in Fig. 7.

The results are presented in Figs. 8–10 (dashed lines). The reference pulse calculated for homogeneous media is drawn with a solid line. As can be observed, if
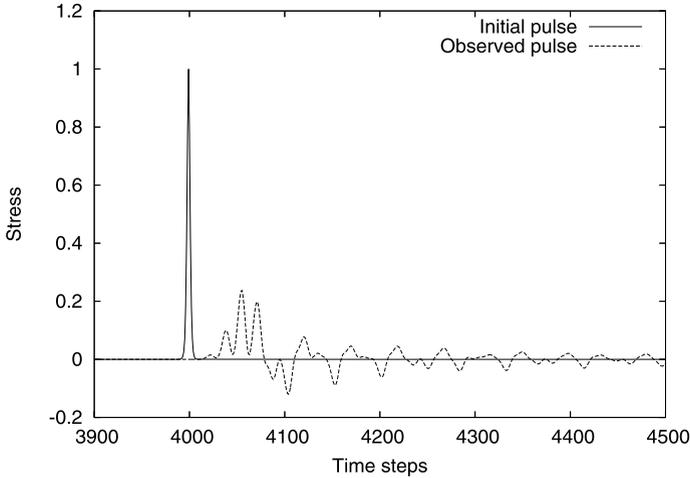
Fig. 10 Pulse shape at 4000 time steps ($d = 8\triangle x, l = 1000\triangle x$).

the wavelength is less then the size of the inhomogeneity ($d \geq \lambda$), we have a strong dispersion of the pulse, i.e., a separation of the wave into components of various frequencies (Figs. 8 and 9). This dispersion is not so strong if, vice versa, the size of the inhomogeneity d is less then the wavelength λ (Fig. 10).

Thus, waves in laminates demonstrate dispersive behavior, which is governed by the relations between the characteristic length scales. Taking into account nonlinear effects, we have seen the soliton-like wave propagation. Both nonlinearity and dispersion effects are observed experimentally in laminates under shock loading.

7 Nonlinear elastic waves in laminates under impact loading

Though the stress response to an impulsive shock loading has been very well understood for homogeneous materials, the same cannot be said for heterogeneous systems. In heterogeneous media, scattering due to interfaces between dissimilar materials plays an important role for shock wave dissipation and dispersion [18].

Diagnostic experiments for the dynamic behavior of heterogeneous materials under impact loading are usually carried out using a plate impact test configuration under a one-dimensional strain state. These experiments were recently reviewed in [12, 13]. For almost all the experiments, the stress response has shown a sloped rising part followed by an oscillatory behavior with respect to a mean value [12, 13]. Such behavior in the periodically layered systems is consistently exhibited in the systematic experimental work [39]. The specimens used in the shock compression experiments [39] were periodically layered two-component composites prepared by repeating a composite unit as many times as necessary to form a specimen with
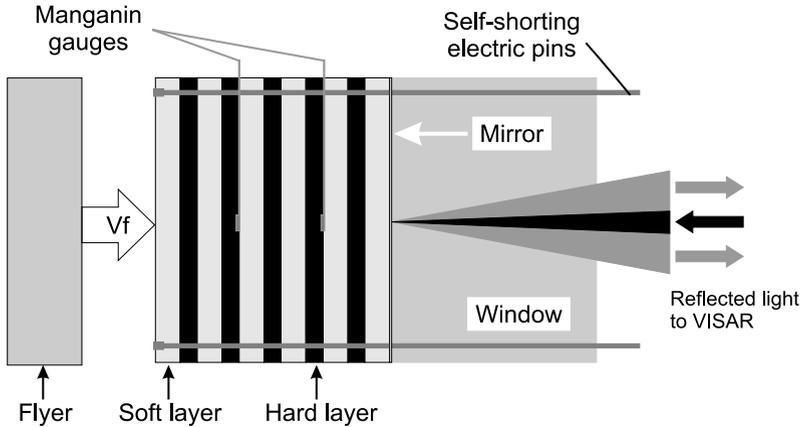
Fig. 11 Experimental setting. Reproduced from [39].

the desired thickness (see Fig. 11). A buffer layer of the same material as the soft component of the specimen was used at the other side of the specimen. A window in contact with the buffer layer was used to prevent the free surface from serious damage due to unloading from shock wave reflection at the free surface. Shock compression experiments were conducted by employing a powder gun loading system, which could accelerate a flat plate flyer to a velocity in the range of 400 m/s to about 2000 m/s. In order to measure the particle velocity history at the specimen window surface, a velocity interferometry system was constructed, and to measure the shock stress history at selected internal interfaces, the manganin stress technique was adopted. Four different materials, polycarbonate, 6061-T6 aluminum alloy, 304 stainless steel, and glass, were chosen as components. The selection of these materials provided a wide range of combinations of shock wave speeds, acoustic impedance and strength levels. The influence of multiple reflections of internal interfaces on shock wave propagation in the layered composites was clearly illustrated by the shock stress profiles measured by manganin gages. The origin of the observed structure of the stress waves was attributed to material heterogeneity at the interfaces. For high velocity impact loading conditions, it was fully realized that material nonlinear effects may play a key role in altering the basic structure of the shock wave.

An approximate solution for layered heterogeneous materials subjected to high velocity plate impact has been developed in [12, 13]. For laminated systems under shock loading, shock velocity, density and volume were related to the particle velocity by means of an equation of state. The elastic analysis was extended to shock response by incorporating the nonlinear effects through computing the shock velocities of the wave trains and superimposing them.

As pointed out in [39], stress wave propagation through layered media made of isotropic materials provides an ideal model to investigate the effect of heterogeneous materials under shock loading, because the length scales, e.g., the thickness of individual layers, and other measures of heterogeneity, e.g., impedance mismatch, are well defined.

Since the impact velocity in shock experiments is sufficiently high, various nonlinear effects may affect the observed behavior. That is why we apply numerical simulations of finite-amplitude nonlinear wave propagation to the study of scattering, dispersion and attenuation of shock waves in layered heterogeneous materials.

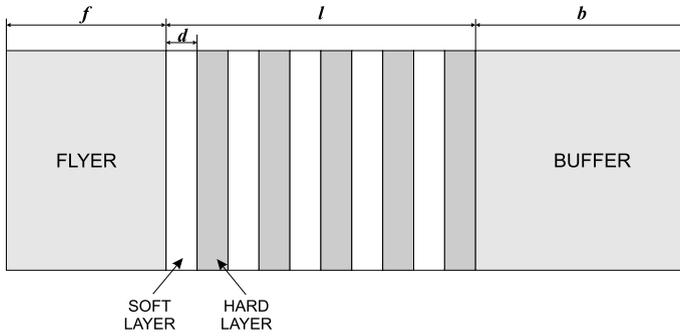The geometry of the problem follows the experimental configuration described in [39] (Fig. 12).

Fig. 12 Geometry of the problem.

We consider the initial-boundary value problem of impact loading of a heterogeneous medium composed of alternating layers of two different materials. The impact is provided by a planar flyer of length L, which has an initial velocity v_0. A buffer of the same material as the soft component of the specimen is used to eliminate the effect of wave reflection at the stress-free surface. The densities of the two materials are different, and the materials' response to compression is characterized by the distinct stress-strain relations $\sigma(\varepsilon)$. Compressional waves propagating in the direction of the layering are modeled by the one-dimensional hyperbolic system of conservation laws (1)–(2).

Initially, stress and strain are zero inside the flyer, the specimen, and the buffer, but the initial velocity of the flyer is nonzero:

$$v(x,0) = v_0, \quad 0 < x < L, \tag{47}$$

where L is the size of the flyer. Both left and right boundaries are stress-free.

Instead of an equation of state like the one used in [12, 13], we apply a simpler nonlinear stress-strain relation $\sigma(\varepsilon,x)$ for each material (43) (cf. [31]):

$$\sigma = \rho c^2 \varepsilon (1 + B\varepsilon), \tag{48}$$

where, as previously, ρ is the density, c is the conventional longitudinal wave speed, and B is a parameter of nonlinearity, the values and signs of which are supposed to be different for hard and soft materials.

We apply the same numerical scheme as in the previous example. The results of the numerical simulations compared with experimental data [39] are presented in the next section.

7.1 Comparison with experimental data

Figure 13 shows the measured and calculated stress time history in the composite, which consists of 8 units of polycarbonate, each 0.74 mm thick, and of 8 units of stainless steel, each 0.37 mm thick. The material properties of the components are extracted from [39]: the density $\rho = 1190$ kg/cm^3 and the sound velocity $c = 1957$ m/s for the polycarbonate; $\rho = 7890$ kg/cm^3 and $c = 5744$ m/s for the stainless steel. The stress time histories correspond to the distance 0.76 mm from the impact face. Calculations are performed for the flyer velocity 561 m/s and the flyer thickness 2.87 mm.
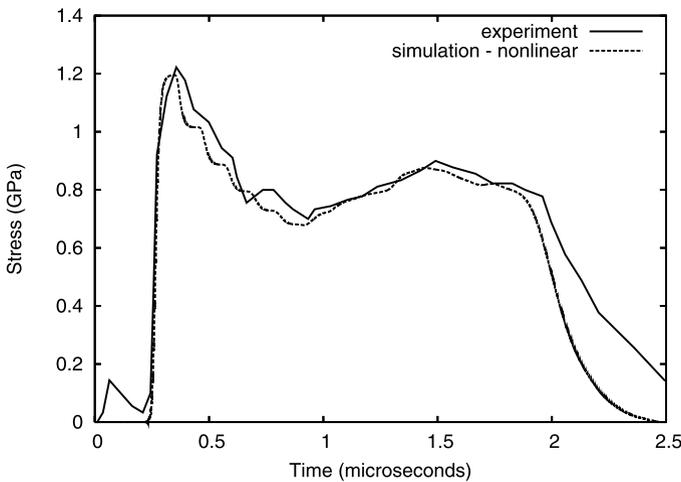

Fig. 13 Comparison of shock stress time histories corresponding to the experiment 112501 [39]. Reproduced from [4].

The results of the numerical calculations depend crucially on the choice of the parameter of nonlinearity B. We choose this parameter from the condition to match the numerical simulations to the experimental results.

Time histories of particle velocity for the same experiment are shown in Fig. 14. It should be noted that the particle velocity time histories correspond to the boundary between the specimen and the buffer. As one can see, both stress and particle velocity time histories are well reproduced by the nonlinear model with the same values of the nonlinearity parameter *B*.
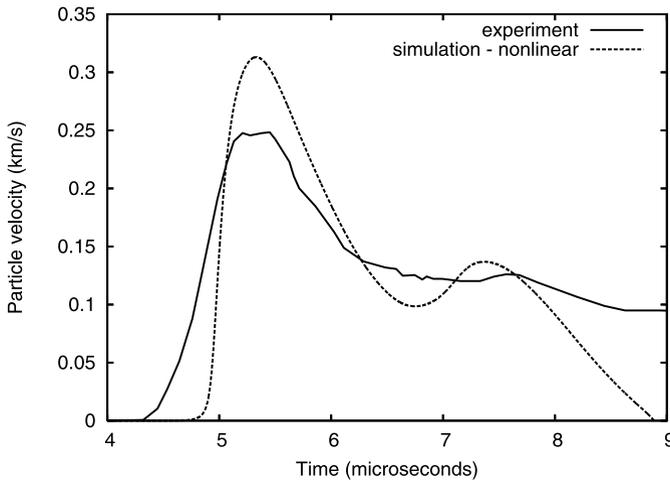

Fig. 14 Comparison of particle velocity time histories corresponding to the experiment 112501 [39]. Reproduced from [4].

As it is pointed out in [39], the influence of multiple reflections of internal interfaces on shock wave propagation in the layered composites is clearly illustrated by the shock stress time histories measured by manganin gages. Therefore, we focus our attention on the comparison of the stress time histories.

Figure 15 shows the stress time histories in the composite, which consists of 16 units of polycarbonate, each 0.37 mm thick, and of 16 units of stainless steel, each 0.19 mm thick. The stress time histories correspond to the distance 3.44 mm from the impact face. Calculations are performed for the flyer velocity 1043 m/s and the flyer thickness 2.87 mm.

The nonlinearity parameter *B* is chosen here to be 2.80 for polycarbonate and zero for stainless steel. Additionally, the stress time history corresponding to the linear elastic solution (i.e., the nonlinearity parameter is zero for both components) is shown. It can be seen that the stress time history computed by means of the considered nonlinear model is very close to the experimental one. It reproduces three main peaks and decreases with distortion, as it is observed in the experiment [39].
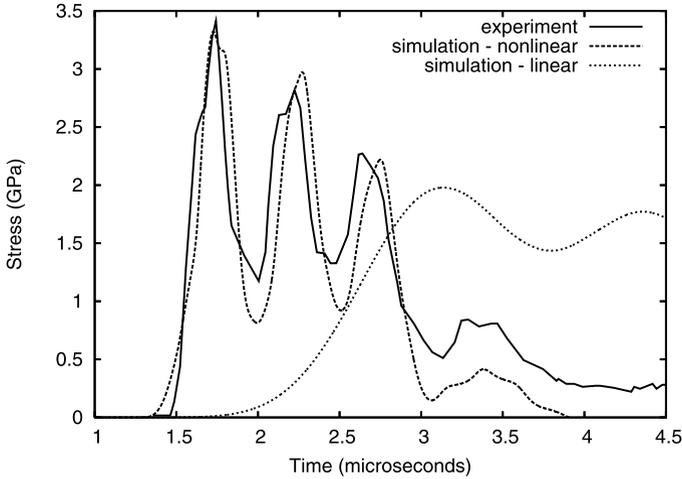
Fig. 15 Comparison of shock stress time histories corresponding to the experiment 110501 [39]. Reproduced from [4].

In Fig. 16 the same comparison is presented for the same composite as in Figure 15, only the flyer thickness is different (5.63 mm). This means that the shock energy is approximately twice as high than that in the previous case. The nonlinearity parameter B is also increased to 4.03 for polycarbonate and remains zero for stainless steel. As a result all 6 experimentally observed peaks are reproduced well.
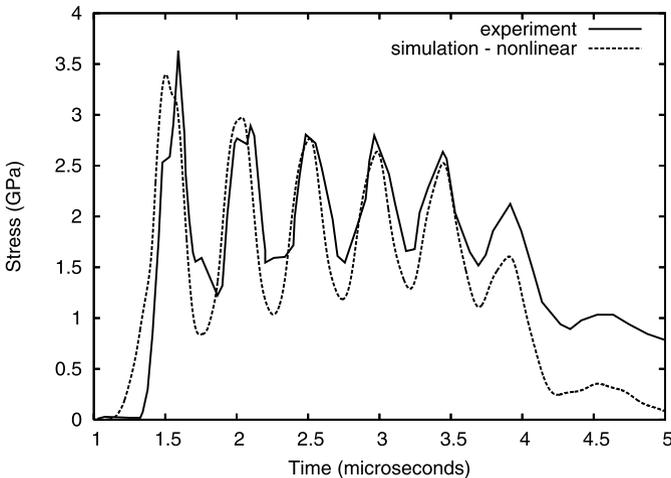

Fig. 16 Comparison of shock stress time histories corresponding to the experiment 110502 [39]. Reproduced from [4].

In Fig. 17 the comparison of stress time histories is presented for the composite consisting of 16 0.37 mm thick units of polycarbonate and 16 0.20 mm thick units of D-263 glass. The material properties of D-263 glass are [39]: the density $\rho = 2510$ kg/cm^3 and the sound velocity $c = 5703$ m/s. The distance between the measurement point and the impact face is 3.41 mm. Corresponding flyer velocity is 1079 m/s and the flyer thickness is 2.87 mm. The nonlinearity parameter B is chosen to be equal 5.025 for polycarbonate and zero for D-263 glass. Again, the stress time history corresponding to the linear elastic solution (i.e., the nonlinearity parameter is zero for both components) is shown. As one can see, the stress time history corresponding to the nonlinear model reproduces all 5 peaks with the same amplitude as observed experimentally.
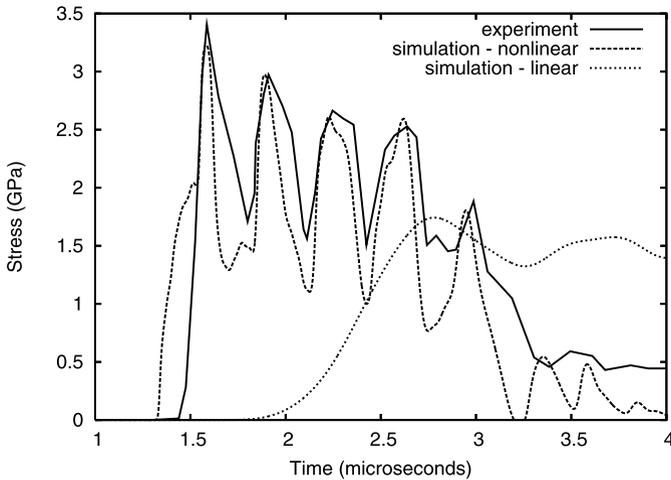

Fig. 17 Comparison of shock stress time histories corresponding to the experiment 112301 [39]. Reproduced from [4].

As it can be seen, the agreement between the results of the calculations and the experiments is achieved by the adjustment of the nonlinearity parameter B.

It follows that the nonlinear behavior of the soft material is affected not only by the energy of the impact, but also by the scattering induced by internal interfaces. It should be noted that the influence of the nonlinearity is not necessarily small. In the numerical simulations, which match with the experiments, the increase of the actual sound velocity of polycarbonate follows. It may be up to two times higher in comparison to the linear case. This conclusion is really surprising, but supported by the stress time histories.

Thus, the application of a nonlinear stress-strain relation for materials in numerical simulations of the plate impact problem of a layered heterogeneous medium shows that a good agreement between computations and experiments can be obtained by adjusting the values of the parameter of nonlinearity [4]. In the numer-

ical simulations of the finite-amplitude shock wave propagation in heterogeneous composites, the flyer size and velocity, the impedance mismatch of hard and soft materials, as well as the number and size of layers in a specimen were the same as in the experiments [39]. Moreover, a nonlinear behavior of materials was also taken into consideration. This means that combining scattering effects induced by internal interfaces and physical nonlinearity in material behavior into one nonlinear parameter, provides the possibility to reproduce the shock response in heterogeneous media observed experimentally. In this context, the parameter B is actually influenced by (i) the physical nonlinearity of the soft material and (ii) the mismatch of the elasticity properties of soft and hard materials. The mismatch effect is similar to the type of nonlinearity characteristic to materials with different moduli of elasticity for tension and compression. The mismatch effect manifests itself due to wave scattering at the internal interfaces, and, therefore, depends on the structure of a specimen. The variation of the parameter of nonlinearity confirms the statement that the nonlinear wave propagation is highly affected by the interaction of the wave with the heterogeneous substructure of a solid [39].

It should be noted that layered media do not exhaust all possible substructures of heterogeneous materials. Another example of a heterogeneous substructure is provided by functionally graded materials.

8 Waves in functionally graded materials

Functionally graded materials (FGMs) are composed of two or more phases that are fabricated so that their compositions vary more or less continuously in some spatial direction and are characterized by nonlinear gradients that result in graded properties. Traditional composites are homogeneous mixtures, and therefore they involve a compromise between the desirable properties of the component materials. Since significant proportions of an FGM contain the pure form of each component, the need for compromise is eliminated. The properties of both components can be fully utilized. For example, the toughness of a metal can be mated with the refractoriness of a ceramic, without any compromise in the toughness of the metal side or the refractoriness of the ceramic side.

Comprehensive reviews of current FGM research may be found in the papers [21] and [30], and in the book [35]. Studies of the evolution of stresses and displacements in FGMs subjected to quasistatic loading [35] show that the utilization of structures and geometry of a graded interface between two dissimilar layers can reduce stresses significantly. Such an effect is also important in the case of dynamical loading, where energy-absorbing applications are of special interest.

We consider the one-dimensional problem in elastodynamics for an FGM slab in which material properties vary only in the thickness direction. It is assumed that the slab is isotropic and inhomogeneous with the following fairly general properties [14]:

$$E'(x) = E_0' \left(a\frac{x}{l} + 1 \right)^m, \quad \rho(x) = \rho_0 \left(a\frac{x}{l} + 1 \right)^n, \tag{49}$$

where ρ is the mass density, l is the thickness, a, m, and n are arbitrary real constants with $a > -1$, while E_0 and ρ_0 are the elastic constant and density at $x = 0$. The elastic constant E_0 is determined under the assumption that $\sigma_{yy} = \sigma_{zz}$ and the slab is fully constrained at infinity. It can thus be shown that

$$E' = \frac{E(1-v)}{(1+v)(1-2v)}, \tag{50}$$

with $E(x)$ and $v(x)$ being the Young modulus and the Poisson ratio of the inhomogeneous material.

It is assumed that the slab is at rest for $t \le 0$, therefore, the following initial conditions are valid:

$$v(x,0) = 0, \quad \sigma(x,0) = 0. \tag{51}$$

The boundary condition at $x = 0$ is

$$v(0,t) = 0, \quad t > 0 \quad \text{(``fixed'' boundary)} \tag{52}$$

At $x = l$, the slab is subjected to a stress pulse given by

$$\sigma_{xx}(l,t) = \sigma_0 f(t), \quad t > 0, \tag{53}$$

where the constant σ_0 is the magnitude of the pulse, the function f describes its time profile, and without any loss in generality, it is assumed that $|f| \le 1$.

Following [14], we consider an FGM slab that consists of nickel and zirconia. The thickness of the slab is $l = 5$ mm. On one surface the medium is pure nickel and on the other surface pure zirconia, while the material properties $E_0(x)$ and $\rho(x)$ vary smoothly in thickness direction. A pressure pulse defined by

$$\sigma_{xx}(l,t) = \sigma_0 f(t) = -\sigma_0(H(t) - H(t-t_0)) \tag{54}$$

is applied to the surface $x = l$ and the boundary $x = 0$ is "fixed". Here H is the Heaviside function. The pulse duration is assumed to be $t_0 = 0.2\,\mu s$. The properties of the constituent materials used are given in Table 1 [14].

Material	E (GPa)	v	ρ (kg/m^3)
ZrO	151	0.33	5331
Ni	207	0.31	8900

Table 1 Properties of materials

The material parameters for the FGMs used are [14]: $a = -0.12354$, $m = -1.8866$, and $n = -3.8866$. The stress is calculated up to $12\,\mu s$ (the propagation time of the plane wave through the thickness $l = 5$ mm is approximately $0.77\,\mu s$ in pure ZrO2 and $0.88\,\mu s$ in Ni).
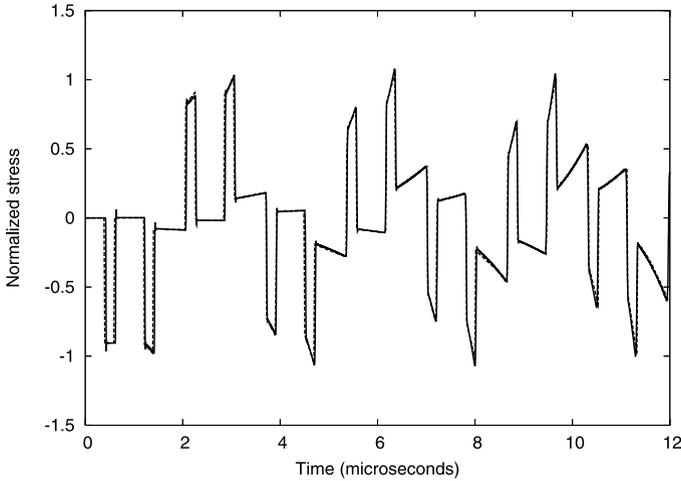
Fig. 18 Variation of stress with time in the middle of the slab. Reproduced from [5].

Numerical simulations were performed by means of the same algorithm as above. The comparison of the results of the numerical simulation and of the analytical solution [14] for the time dependence of the normalized stress σ_{xx}/σ_0 at the location $x/l = 1/2$ is shown in Fig. 18.

As one can see, it is difficult to make a distinction between analytical and numerical results. This means that the applied algorithm is well suited for the simulation of wave propagation in FGM.

A nonlinear behavior for the same materials with the nonlinearity parameter $A = 0.19$ is shown in Figure 19. For the comparison, calculations were performed with the value 0.9 of the Courant number both in the linear and nonlinear case. The amplitude amplification and pulse shape distortion in comparison with the linear case is clearly observed. In addition, the velocity of a pulse in the nonlinear material is increased.

9 Concluding remarks

As we have seen, linear and non-linear wave propagation in media with rapidly-varying properties as well as in functionally graded materials can be successfully simulated by means of the modification of the wave-propagation algorithm based on the non-equilibrium jump relation for true inhomogeneities. It should be emphasized that the used jump relation expresses the continuity of genuine unknown fields at the boundaries between computational cells. The applied algorithm is conservative, stable up to Courant number equal to 1, high-order accurate, and thermodynamically consistent. However, the main advantage of the presented modification of
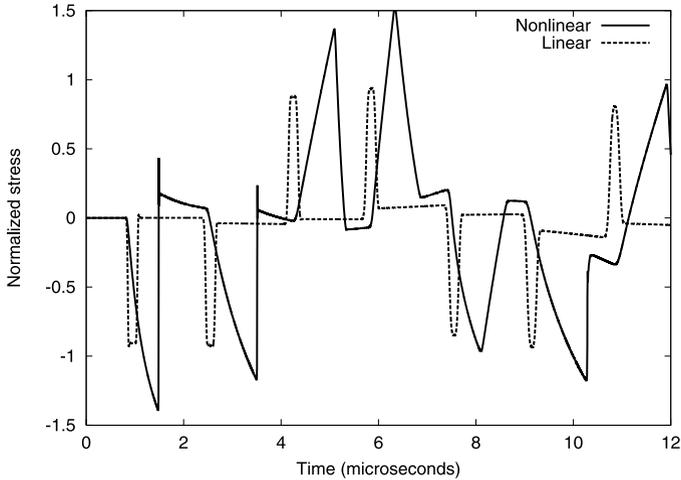
Fig. 19 Variation of stress with time in the middle of the slab. Nonlinear case. Reproduced from [5].

the wave-propagation algorithm is its applicability to the simulation of moving discontinuities. This property is related to the formulation of the algorithm in terms of excess quantities. To apply the algorithm to moving singularities, we simply should change the non-equilibrium jump relation for true inhomogeneities to another non-equilibrium jump relation valid for quasi-inhomogeneities.

References

1. Achenbach, J.D.: Wave Propagation in Elastic Solids. North-Holland, Amsterdam (1973)
2. Bale, D.S., LeVeque, R.J., Mitran, S., Rossmanith, J.A.: A wave propagation method for conservation laws and balance laws with spatially varying flux functions. SIAM J. Sci. Comp. **24**, 955–978 (2003)
3. Bedford, A., Drumheller, D.S.: Introduction to Elastic Wave Propagation. Wiley, New York (1994)
4. Berezovski, A., Berezovski, M., Engelbrecht, J.: Numerical simulation of nonlinear elastic wave propagation in piecewise homogeneous media. Mater. Sci. Eng. **A418**, 364–369 (2006)
5. Berezovski A, Berezovski, M., Engelbrecht, J., Maugin, G.A.: Numerical simulation of waves and fronts in inhomogeneous solids. In: Nowacki, W.K., Zhao, H. (eds.) Multi-Phase and Multi-Component Materials under Dynamic Loading, pp. 71-80. Inst. Fundam. Technol. Research, Warsaw (2007)
6. Berezovski, A., Maugin, G.A.: Simulation of thermoelastic wave propagation by means of a composite wave-propagation algorithm. J. Comp. Physics **168**, 249–264 (2001)

7. Berezovski, A., Maugin, G.A.: Thermoelastic wave and front propagation. J. Thermal Stresses **25**, 719–743 (2002)
8. Berezovski, A., Maugin, G.A.: Stress-induced phase-transition front propagation in thermoelastic solids. Eur. J. Mech. A/Solids **24**, 1–21 (2005)
9. Billingham, J., King, A.C.: Wave Motion. Cambridge University Press (2000)
10. Chakraborty, A., Gopalakrishnan, S.: Various numerical techniques for analysis of longitudinal wave propagation in inhomogeneous one-dimensional waveguides. Acta Mech. **162**, 1–27 (2003)
11. Chakraborty, A., Gopalakrishnan, S.: Wave propagation in inhomogeneous layered media: solution of forward and inverse problems. Acta Mech. **169**, 153–185 (2004)
12. Chen, X., Chandra, N.: The effect of heterogeneity on plane wave propagation through layered composites. Comp. Sci. Technol. **64**, 1477–1493 (2004)
13. Chen, X., Chandra, N., Rajendran, A.M.: Analytical solution to the plate impact problem of layered heterogeneous material systems. Int. J. Solids Struct. **41**, 4635–4659 (2004)
14. Chiu, T.-C., Erdogan, F.: One-dimensional wave propagation in a functionally graded elastic medium. J. Sound Vibr. **222**, 453–487 (1999)
15. Engelbrecht, J., Berezovski, A., Pastrone, F., Braun, M.: Waves in microstructured materials and dispersion. Phil. Mag. **85**, 4127–4141 (2005)
16. Fogarthy, T., LeVeque, R.J.: High-resolution finite-volume methods for acoustics in periodic and random media. J. Acoust. Soc. Am. **106**, 261–297 (1999)
17. Godlewski, E., Raviart, P.-A.: Numerical Approximation of Hyperbolic Systems of Conservation Laws. New York, Springer (1996)
18. Grady, D.: Scattering as a mechanism for structured shock waves in metals. J. Mech. Phys. Solids **46**, 2017–2032 (1998)
19. Graff, K.F.: Wave Motion in Elastic Solids. Oxford University Press (1975)
20. Guinot, V.: Godunov-type Schemes: An Introduction for Engineers. Elsevier, Amsterdam (2003)
21. Hirai, T.: Functionally graded materials. In: Processing of Ceramics. Vol. 17B, Part 2, pp. 292-341. VCH Verlagsgesellschaft, Weinheim (1996)
22. Hoffmann, K.H., Burzler, J.M., Schubert, S.: Endoreversible thermodynamics. J. Non-Equil. Thermodyn. **22**, 311–355 (1997)
23. Langseth, J.O., LeVeque, R.J.: A wave propagation method for three-dimensional hyperbolic conservation laws. J. Comp. Physics **165**, 126–166 (2000)
24. LeVeque, R.J.: Wave propagation algorithms for multidimensional hyperbolic systems. J. Comp. Physics **131**, 327–353 (1997)
25. LeVeque, R.J.: Balancing source terms and flux gradients in high-resolution Godunov methods: the quasi-steady wave-propagation algorithm. J. Comp. Physics **148**, 346–365 (1998)
26. LeVeque, R.J.: Finite volume methods for nonlinear elasticity in heterogeneous media. Int. J. Numer. Methods in Fluids **40**, 93–104 (2002)
27. LeVeque, R.J.: Finite Volume Methods for Hyperbolic Problems. Cambridge University Press (2002)
28. LeVeque, R.J., Yong, D.H.: Solitary waves in layered nonlinear media. SIAM J. Appl. Math. **63**, 1539–1560 (2003)
29. Liska, R., Wendroff, B.: Composite schemes for conservation laws. SIAM J. Numer. Anal. **35**, 2250–2271 (1998)
30. Markworth, A.J., Ramesh, K.S., Parks, W.P.: Modelling studies applied to functionally graded materials. J. Mater. Sci. **30**, 2183–2193 (1995)
31. Meurer, T., Qu, J., Jacobs, L.J.: Wave propagation in nonlinear and hysteretic media – a numerical study. Int. J. Solids Struct. **39**, 5585–5614 (2002)
32. Muschik, W., Berezovski, A.: Thermodynamic interaction between two discrete systems in non-equilibrium. J. Non-Equilib. Thermodyn. **29**, 237–255 (2004)
33. Rokhlin, S.I., Wang, L.: Ultrasonic waves in layered anisotropic media: characterization of multidirectional composites. Int. J. Solids Struct. **39**, 5529–5545 (2002)
34. Santosa, F., Symes, W.W.: A dispersive effective medium for wave propagation in periodic composites. SIAM J. Appl. Math. **51**, 984–1005 (1991)

35. Suresh, S., Mortensen, A.: Fundamentals of Functionally Graded Materials. The Institute of Materials, IOM Communications, London (1998)
36. Toro, E.F.: Riemann Solvers and Numerical Methods for Fluid Dynamics. Springer, Berlin (1997)
37. Toro, E.F. (ed.): Godunov Methods: Theory and Applications. Kluwer, New York (2001)
38. Wang, L., Rokhlin, S.I.: Recursive geometric integrators for wave propagation in a functionally graded multilayered elastic medium. J. Mech. Phys. Solids **52**, 2473–2506 (2004)
39. Zhuang, S., Ravichandran, G., Grady, D.: An experimental investigation of shock wave propagation in periodically layered composites. J. Mech. Phys. Solids **51**, 245–265 (2003)